Convective heat transfer as a function of wavelength: Implications for the cooling of the Earth

C. Grigné
Department of Earth and Space Sciences, University of California, Los Angeles, California, USA

S. Labrosse
Institut de Physique du Globe de Paris, Paris, France

P. J. Tackley
Department of Earth and Space Sciences, University of California, Los Angeles, California, USA

Received 4 August 2004; revised 5 November 2004; accepted 19 November 2004; published 26 March 2005.

[1] Attempting to reconstruct the thermal history of the Earth from a geophysical point of view has for a long time been in disagreement with geochemical data. The geophysical approach uses parameterized models of mantle cooling. The rate of cooling of the Earth at the beginning of its history obtained in these models is generally too rapid to allow a sufficient present-day secular cooling rate. Geochemical estimates of radioactive element concentrations in the mantle then appear too low to explain the observed present mantle heat loss. Cooling models use scaling laws for the mean heat flux out of the mantle as a function of its Rayleigh number of the form $Q \propto Ra^{\beta}$. Recent studies have introduced very low values of the exponent β, which can help reduce the cooling rate of the mantle. The present study instead focuses on the coefficient C in the relation $Q = C\,Ra^{\beta}$ and, in particular, on its variation with the wavelength of convection. The heat transfer strongly depends on the wavelength of convection. The length scale of convection in Earth's mantle is that of plate tectonics, implying convective cells of wide aspect ratio. Taking into account the long wavelength of convection in Earth's mantle can significantly reduce the efficiency of heat transfer. The likely variations of this wavelength with the Wilson cycle thus imply important variations of the heat flow out of the Earth on a intermediate timescale of 100 Ma, which renders parameterized models of thermal evolution inaccurate for quantitative predictions.

Citation: Grigné, C., S. Labrosse, and P. J. Tackley (2005), Convective heat transfer as a function of wavelength: Implications for the cooling of the Earth, *J. Geophys. Res.*, *110*, B03409, doi:10.1029/2004JB003376.

1. Introduction

[2] Scaling laws of the form $Q \propto Ra^{\beta}$, where Q is the mean heat flux out of the fluid and Ra the Rayleigh number of the fluid, are often used for the thermal history of the Earth [e.g., *Schubert et al.*, 1980; *Davies*, 1980]. For an isoviscous fluid, a boundary layer analysis gives an exponent $\beta = 1/3$. Two main heat sources must explain the present observed mean heat flux at the surface of the Earth: the production of heat by decay of radioactive elements, and the secular cooling of the mantle. The first term is traditionally written using the Urey ratio, defined as the ratio between the heat production by radioactive elements within the mantle and the total heat loss of the mantle. For whole mantle convection, geochemical estimates [e.g., *Jochum et al.*, 1983; *Allègre et al.*, 1988] give a present Urey ratio around 0.4. With a radioactive heat production corresponding to this Urey ratio, simple parameterized models of mantle convection lead to a cooling of the Earth at the beginning of its history that is too fast (rapid initial cooling) and they are unable to explain the present heat loss of the Earth. Using a scaling of the form $Q \sim Ra^{1/3}$, *Schubert et al.* [1980] concluded that Urey ratios that lead to the present-day heat flux being satisfied are between 0.65 and 0.85, values significantly higher than what is given by geochemical estimates.

[3] Early studies proposed to solve this discrepancy by reducing the exponent β in the relation $Q \sim Ra^{\beta}$, in order to slow down the cooling rate of the mantle and increase the sensitivity to initial conditions. With an exponent of 1/3, the balance between internal heat production and efficiency of heat transfer for a mantle with a temperature-dependent viscosity is such that the system is not sensitive to the initial conditions and self-regulates at each time step [*Tozer*, 1972]: a local increase in heat production results in a lower viscosity, and thus in more vigorous convection, that carries away this excess heat. With an exponent β smaller than 1/3, this self-regulation is reduced and the rate of cooling becomes sensitive to the initial conditions. *Christensen*

0148-0227/05/2004JB003376$09.00

[1985] proposed an exponent $\beta \sim 0.1$ for models with a temperature-dependent viscosity. It was, however, shown by *Davaille and Jaupart* [1993] and *Solomatov* [1995] that this low value of β was obtained only for the transitional regime between the small viscosity contrast regime and the stagnant lid one. Furthermore, the Earth's mantle is not in the stagnant lid regime. *Gurnis* [1989] showed that for models with a strongly temperature-dependent viscosity, but in which the lid is mobilized in a plate-like regime, the value of β is close to 1/3. *Honda* [1997] emphasized too that weak margins introduced into a model with a strongly temperature-dependent viscosity enhanced the efficiency of the heat transfer, rendering it similar to the isoviscous case. Temperature dependence of the viscosity alone cannot solve the problem of the cooling of the mantle.

[4] Recent studies have introduced complex physical processes to obtain low values of the exponent β. *Conrad and Hager* [1999] proposed that plate tectonic rate, and consequently heat transfer, is controlled mainly by plate bending in subduction zones, leading to a weak dependence of the heat flow on the mantle viscosity and temperature. They therefore proposed an exponent $\beta < 0.1$. In subsequent numerical experiments [*Conrad and Hager*, 2001], they, however, obtained values of β over 0.15, and this value of 0.15 was obtained only if a low viscosity asthenosphere was placed under the lithospheric plate. Values of β smaller than 1/3 were, however, obtained under certain conditions, and can help to slow down the cooling rate of the mantle. In models introducing the effect of dehydration of the mantle during melting, *Korenaga* [2003] argues that a hotter mantle results in a deeper onset of melting, and thus in a thicker and stiffer lithosphere, which reduces the heat loss. Above a given temperature, this effect becomes more important than the fact that a higher temperature results in a less viscous mantle, more vigorous convection and higher heat flows. The mean heat flux can then decrease with increasing mantle temperature. Using a scaling law with a temperature- and depth-dependent viscosity, *Korenaga* [2003] finally obtains $\beta \sim -0.15$. With such an exponent, satisfactory models of Earth cooling can be obtained even for low present-day Urey ratios.

[5] The scaling for the surface heat flux, $Q = C\,Ra^{\beta}$, gives a dimensional form $q = C\,(k\,\Delta T/d)Ra^{\beta} \propto C\,\mu^{-\beta}\,(\Delta T)^{\beta+1}\,d^{3\beta-1}$, which makes clear the effect of β on the self-regulation mechanism proposed by *Tozer* [1972]. On the other hand, for convection at high Rayleigh number, where the dynamics of the boundary layer is largely unaffected by the rest of the flow, one can expect the heat flux at the surface to be independent of the total depth d of the system [*Kraichnan*, 1962]. The dimensional form of $q = f(Ra)$ shows that this condition can be attained only for an exponent $\beta = 1/3$.

[6] In the present study, the simple context of Rayleigh-Bénard convection is first considered, to address a question that has received no attention in parameterized models of convection, which is the dependence of the heat flux on the wavelength of convection. Rather than focusing on the exponent β in the relation $Q = C\,Ra^{\beta}$, we focus on the prefactor C and on its dependence on the length scale of convection, and we propose a simple alternative solution to decrease the heat transfer efficiency in the mantle. Cooling models for the mantle do not consider explicitly the geometry of the flow and use parameterizations that were obtained in situations where the dominant horizontal wavelength of convection is close to the depth of the system (cells of aspect ratio one). Convection in the Earth is of long wavelength. Presently, there are two main zones of subduction in the mantle, on each side of the Pacific Ocean, and two large zones of upwelling, under Africa and under the Central Pacific. The general view that mantle convection is dominated by long wavelengths, and that this characteristic is not an effect of a poor observation of short wavelengths, is now largely accepted [*Hager et al.*, 1985; *Su and Dziewonski*, 1991; *Woodward and Masters*, 1991; *Zhang and Tanimoto*, 1991; *Montagner*, 1994]. The wavelength of convection in Earth's mantle is thus to first order the one of plate tectonics, with sublinear regions of downwelling along subduction zones and regions of divergence along ridges. This pattern is acceptably well represented by a two-dimensional cellular circulation, with convective cells of aspect ratio close to 3 for the present-day mantle.

[7] Heat transfer by convection depends on the horizontal wavelength of the flow. For convective cells of aspect ratio larger than one, the mean heat flux decreases with the size of the cells [e.g. *Turcotte and Oxburgh*, 1967; *Turcotte and Schubert*, 1982, 2002]. *Zhong and Gurnis* [1994], using numerical models of convection where plates are generated by the use of imposed surface velocities and a temperature-dependent viscosity, obtained a systematic decrease of the mean heat flux at the surface of the model with increasing plate size, with a mean heat flux that can be reduced by 50% for plates whose size L is 5 times the depth d of the model, compared to plates of size $L = d$. *Lowman et al.* [2001] addressed a similar question and also obtained a significant decrease of the mean heat flux as a function of the plate size. Using parameterizations that are derived from results at aspect ratio one for models of cooling of the Earth can lead to an overestimate of the heat transfer efficiency in the mantle.

[8] In order to quantify the relation between the heat flux and the wavelength of convection, simple models of Rayleigh-Bénard convection are first considered, and the effect of a variable wavelength is studied in an isolated way, independent of any other level of complexity. A more complex rheology is introduced in section 4 in order to attain large size convection cells. A simple fluid loop model [e.g., *Turcotte and Schubert*, 1982] is first derived to help and interpret the results of full computations of models of convection, which are presented afterward.

2. Fluid Loop Model

[9] In simple models of convection, the notion of convective cells is obvious at low Rayleigh numbers. Figure 1 shows an example of Rayleigh-Bénard convection at a Rayleigh number of 10^5. Four cells of aspect ratio one are clearly present in the box. This notion of cells is less clear at high Rayleigh numbers, where convection is highly non-stationary. Two snapshots of the temperature field obtained at $Ra = 10^8$ are presented in Figure 2, for Rayleigh-Bénard convection in two dimensions. Two kinds of plumes can be seen in the model: long plumes, crossing the whole depth of the fluid, with a relatively steady position (large triangles in Figure 2), and smaller plumes, attracted toward the larger

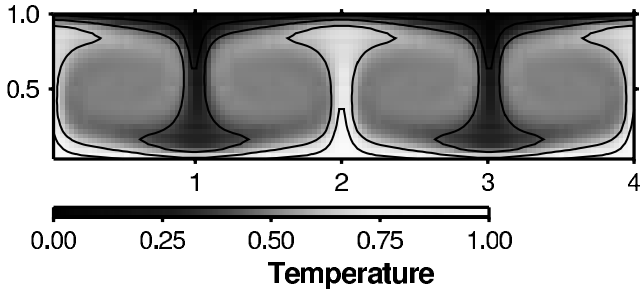

Figure 1. Temperature field for a Rayleigh-Bénard convection at $Ra = 10^5$.

subvertical plumes (small triangles in Figure 2). Even though instantaneous temperature fields do not appear as simple cells, the attraction of small plumes toward the larger plumes defines a cellular circulation.

[10] We use an approach similar to the one used by *Turcotte and Oxburgh* [1967] and *Turcotte and Schubert* [1982, 2002] to build a loop model of convection, but bring two modifications that substantially improve the agreement between the loop model and the heat flux observed in numerical calculations of Rayleigh-Bénard convection. We consider two-dimensional steady state convection. The core of the convective cell is well mixed and is considered to have a homogeneous temperature T_i. Heat is transferred through the horizontal boundary layers on top and at the base of the cell by conduction. The vertical limits of the cell are the cold downwelling and hot upwelling, both considered to be strictly vertical, and separated by the cell width L. A schematic drawing in Figure 3 indicates the notations used. The horizontal velocity u on top and at the base of the fluid, and the vertical velocity w in the upwellings and downwellings, both referred to as "plumes" in the remainder of this paper, are considered to be uniform along the respective sides of the cell.

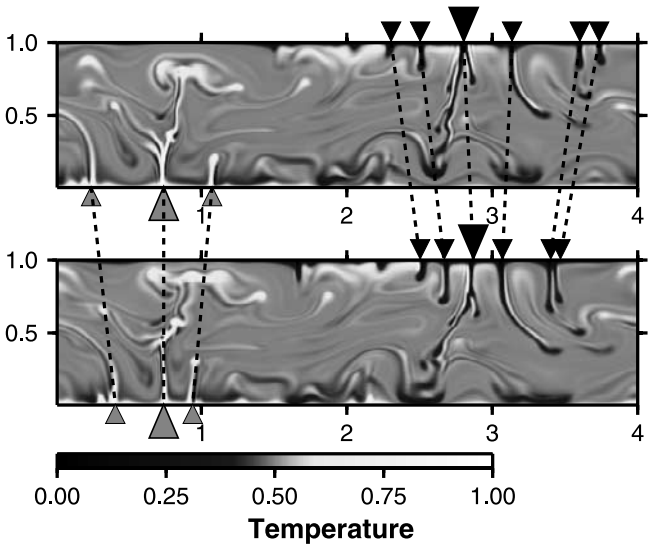

Figure 2. Temperature field for Rayleigh-Bénard convection at $Ra = 10^8$, at two different time steps. Small triangles follow plumes moving toward steadier and larger plumes (larger triangles).

[11] We first consider the distribution of the temperature T in the horizontal boundary layers. A model of cooling by conduction of a half-space is used, which yields for the upper boundary layer:

$$\frac{T_i - T(x,z)}{T_i - T_0} = \mathrm{erfc}\left[\frac{z}{2}\left(\frac{u}{\kappa x}\right)^{1/2}\right], \tag{1}$$

where T_0 is the fixed temperature imposed at the surface of the fluid and κ is the thermal diffusivity of the fluid. The heat flux at the surface of the fluid can then be computed:

$$q_t(x) = k\left(\frac{\partial T}{\partial z}\right)_{z=0} = k\ (T_i - T_0)\ \left(\frac{u}{\pi\kappa x}\right)^{1/2}, \tag{2}$$

where k is the thermal conductivity of the fluid. The mean heat flux is then:

$$\overline{q_t} = \frac{1}{L}\int_0^L q_t(x)\ dx = 2k\ (T_i - T_0)\ \left(\frac{u}{\pi\kappa\ L}\right)^{1/2}. \tag{3}$$

[12] To compute the horizontal velocity u, the equilibrium between the work of the driving force of convection and the work of the resisting force is written. The driving force is the buoyancy force of the plumes. The method we use to compute it differs substantially from the one used by *Turcotte and Schubert* [1982, 2002], which appears to lead to a heat flux that is too high compared to the observations. On each side of the cell, we consider half plumes, with δ as mean thermal width. We denote by T_c the mean temperature of the cold plume. The buoyancy force of the half cold plume can be written:

$$f_c = \alpha\ \rho_0 g\ \delta\ (T_i - T_c), \tag{4}$$

with α the coefficient of thermal expansion, ρ_0 the reference density and g the gravitational acceleration. The half cold plume carries the following heat rate per unit of length:

$$A_c = \rho_0 C_p\ w\ \delta\ (T_i - T_c). \tag{5}$$

[13] The hot and cold plumes are considered to be perfectly symmetrical to each other. Each half plume must

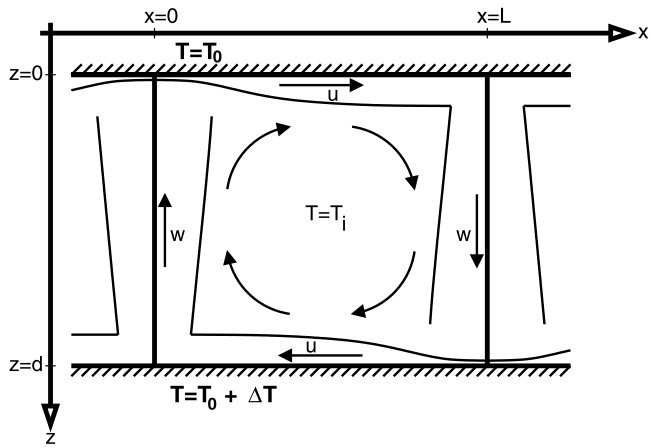

Figure 3. Loop model for a convective cell of width L and height d [from *Turcotte and Oxburgh*, 1967](with permission from Cambridge University Press).

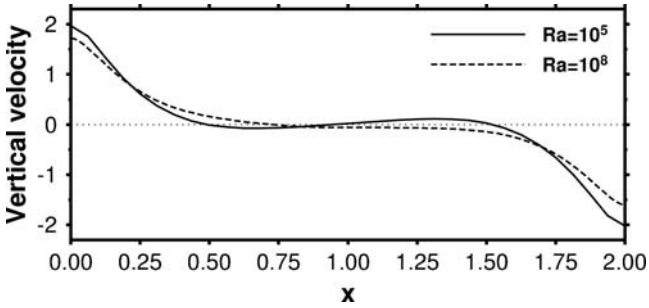

Figure 4. Profiles of observed mean vertical velocity at $Ra = 10^5$ and $Ra = 10^8$ at middepth of the model. Velocities are normalized using the root mean square of the velocity.

then carry half of the total heat going out of the cell $\overline{q_t}\ L$. This gives, using equation (3),

$$A_c = k\ (T_i - T_0)\ \left(\frac{u}{\pi\kappa\ L}\right)^{1/2} L. \tag{6}$$

Equating (5) and (6) gives

$$\delta\ (T_i - T_c) = \kappa\ (T_i - T_0)\ \frac{u}{w}\ \left(\frac{L}{u\ \pi\kappa}\right)^{1/2}, \tag{7}$$

which can be reintroduced in equation (4), and finally gives the buoyancy force of the cold plume:

$$f_c = \alpha\ \rho_0 g\ (T_i - T_0)\ \frac{u}{w}\ \left(\frac{\kappa L}{u\ \pi}\right)^{1/2}. \tag{8}$$

[14] To compute the viscous shear stresses, we consider a linear vertical profile for the horizontal velocity. For the vertical velocity, the form obtained in the models constructed during the present study is always similar to the one presented in Figure 4. The profiles in Figure 4 are obtained from numerical computations, using the method described in Appendix A to construct mean convective cells. They indicate that the form of the vertical velocity is not linear along the width of the cell. This characteristic was already noticed by *Jarvis and Peltier* [1982], who noted that the horizontal gradient of the vertical velocity clearly increases closer to the vertical plumes. A large number of experiments have been carried out during the present study, at Rayleigh numbers between 10^5 and 10^8 for different aspect ratios of the model, which lead to various cell widths. It appears that the velocity is nonnegligible on a width which, to first order, does depend neither on the Rayleigh number, nor on the cell width. This width is close to the half depth of the model.

[15] The profiles of horizontal and vertical velocities used in our loop model are presented in Figure 5. To correct the loop model by *Turcotte and Schubert* [1982, 2002], which uses a linear profile of vertical velocity, we introduce the parameter λ that defines the constant width described above, on which the vertical velocity presents nonnegligible variations: $\lambda \sim 0.5\ d$.

[16] Considering a uniform viscosity μ, these profiles lead to a horizontal shear stress:

$$\tau_h = \mu\left(\frac{\partial u}{\partial z}\right) = \mu\ \frac{2u}{d}, \tag{9}$$

and to a vertical shear stress:

$$\tau_v = \mu\left(\frac{\partial w}{\partial x}\right) = \mu\ \frac{w}{\lambda}. \tag{10}$$

These profiles also yield the following equation for the conservation of mass:

$$u\ \frac{d}{2} = w\ \lambda. \tag{11}$$

[17] The equilibrium between the work of these shear stresses and the buoyancy forces of the plumes is:

$$w\ f_c\ d + w\ f_h\ d = 2u\ L\ \tau_h + 2w\ d\ \tau_v, \tag{12}$$

where f_c and f_h are the buoyancy forces respectively of the cold and hot plumes. The two plumes are considered to be symmetrical: $f_c = f_h$. Equations (8) and (12), with the shear stresses given by equations (9)–(10), lead to

$$\frac{\alpha\rho_0 g\Delta T d^3}{\kappa\mu}\left(\frac{\kappa}{d}\right)^{3/2}\frac{T_i - T_0}{\Delta T}\left(\frac{u\ L}{\pi\ d}\right)^{1/2} = 2u^2\frac{L}{d} + w^2\frac{d}{\lambda}. \tag{13}$$

[18] Introducing the Rayleigh number,

$$Ra = \frac{\alpha\rho_0 g\ \Delta T\ d^3}{\kappa\mu} \tag{14}$$

and using the mass conservation (equation (11)), we obtain:

$$u = \frac{\kappa}{d}\left(\frac{Ra}{2\sqrt{\pi}}\right)^{2/3}\left(\frac{T_i - T_0}{\Delta T}\right)^{2/3}\frac{(L/d)^{1/3}}{\left(\frac{L}{d} + \frac{d^3}{8\lambda^3}\right)^{2/3}}. \tag{15}$$

[19] This horizontal velocity can be reintroduced in equation (3), and the mean heat flux can be written:

$$\overline{q_t} = k\left(\frac{2}{\pi}\right)^{2/3}\frac{Ra^{1/3}}{d^{2/3}}\frac{(T_i - T_0)^{4/3}}{\Delta T^{1/3}}\frac{1}{L^{1/3}\left(\frac{L}{d} + \frac{d^3}{8\lambda^3}\right)^{1/3}}. \tag{16}$$

[20] Using the depth d of the fluid as the characteristic length and the jump of temperature ΔT as the characteristic

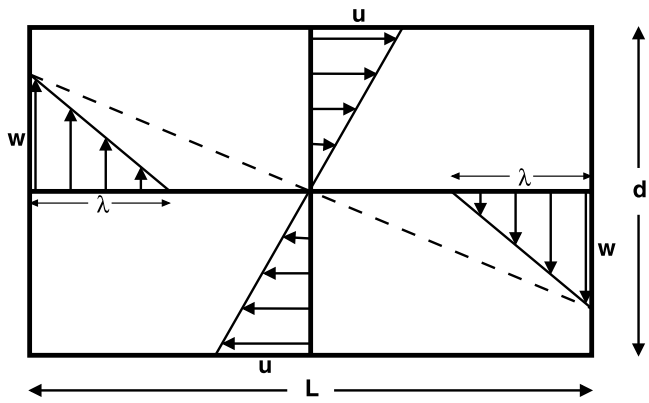

Figure 5. Model of velocity profiles used in this study. The dashed line represents the linear profile used by *Turcotte and Schubert* [1982, 2002].

temperature for the nondimensionalization, the mean heat flux in a dimensionless form is

$$Q = \left(\frac{2}{\pi}\right)^{2/3} Ra^{1/3} \frac{(T_i - T_0)^{4/3}}{\left(L^2 + \frac{L}{8\lambda^3}\right)^{1/3}}. \quad (17)$$

[21] This expression differs from the one given by *Turcotte and Schubert* [1982, 2002]:

$$Q_{TS} = \frac{2}{\pi^{2/3}} Ra^{1/3} \frac{(T_i - T_0)^{4/3}}{(L^2 + L^{-2})^{1/3}}. \quad (18)$$

Two modifications have been introduced. The first one concerns the computation of the buoyancy forces of the plumes. *Turcotte and Schubert* [1982, 2002] consider that the fluid in the thermal boundary layer simply undergoes a 90° rotation at the cell corner, with no thermal diffusion or complexity in the velocity field. The buoyancy flux being conserved by fluid motion in the plume, they use the temperature profile in the boundary layer to compute this buoyancy flux. They also consider a horizontal velocity in the corner of the cell equal to the one above the center of the cell. This leads to the heat transported by vertical advection through the cell interior being larger than the one transported by conduction through the upper or lower boundary, so thermal energy is not conserved.

[22] However, the horizontal velocity drops above the cold plume, and the dynamics of the corner flow are somewhat more complex than a 90° rotation. In the present paper, the distribution of temperature in the horizontal boundary layers is used to compute the buoyancy forces of the plumes (equations (4)–(8)) such that the heat advected by the plumes at middepth is equal to the heat conducted through the boundary layers, ensuring that the global conservation of energy is respected. The buoyancy force we thus compute is two times smaller than the one obtained by *Turcotte and Schubert* [1982, 2002].

[23] The second modification concerns the horizontal profiles of the vertical velocity. *Turcotte and Schubert* [1982, 2002] do not use profiles of the form of the ones presented in Figure 4, but linear profiles, for all Rayleigh numbers and all cell widths. With the notation used in this study, it is equivalent to $\lambda = L/2$, and leads to a dependence of the heat flux Q on the width of the cell L which is $(L^2 + L^{-2})^{-1/3}$ in equation (18), instead of $(L^2 + L/(8\lambda^3))^{-1/3}$ in equation (21).

3. Simple Rayleigh-Bénard Convection

[24] Two-dimensional numerical experiments of thermal convection have been carried out. Equations of convection for an isoviscous fluid at infinite Prandtl number were solved using the code Stag [e.g., *Tackley*, 1993], in a Cartesian geometry. The mechanical boundary conditions were zero shear stress on the horizontal boundaries, and periodicity on the vertical boundaries of the model. Experiments were carried out for Rayleigh numbers ranging from 10^4 to 10^8. Models cover a large range of aspect ratios, in order to obtain various widths of convective cells.

[25] We aim to study the heat transfer as a function of the wavelength of convection. In order to do so, we must be able to define cells of convection at all Rayleigh numbers. We indicated that the notion of cells is not obvious at high Rayleigh numbers (see Figure 2). Convection at high Rayleigh numbers is highly nonstationary, and plumes move with time. A numerical method, using an approach in the same spirit as *Labrosse* [2002] but with some differences that are presented in Appendix A, was implemented to detect plumes and operate a stacking of convective cells over time. Mean synthetic cells, describing the general cellular circulation in the model, are thus constructed. This method is described in Appendix A. It allows us to study the heat transfer as a function of the wavelength of convection at all Rayleigh numbers.

[26] One must keep in mind the fact that with periodic boundary conditions on the vertical walls of the model, the model must contain an even number of cells. In most cases, the model preferentially adopts a pattern of convection with cells of aspect ratio close to one. It is then straightforward to obtain cells of aspect ratio up to 1.5, simply using models of aspect ratio smaller than 3. Wider cells can be obtained at low Rayleigh numbers, up to 10^5, in a steady state. They can also be obtained as a transitory state at higher Rayleigh numbers. At Rayleigh numbers of 10^6, 10^7 and 10^8, in a model of aspect ratio 4, the pattern of convection varies regularly between two cells of aspect ratio 2 and four cells of aspect ratio 1. An example is shown in Figures A1 and A2 in Appendix A. It was possible to obtain, at least transiently, cells of aspect ratio up to 3 at Rayleigh number up to 10^6, slightly larger than 2 at $Ra = 10^7$ and close to 2 at $Ra = 10^8$.

[27] Even though the question of the selection of the wavelength of convection is not assessed precisely in this study, it is to be noted that the often used argument asserting that the selected pattern of convection is the one which gives the most efficient heat transfer is not verified here. The scaling law given by equation (21) predicts a maximum heat flux for cells of aspect ratio 2λ, that is to say close to 1. Cells of aspect ratio 1 seem indeed easy to obtain, but the geometry of the model is also an important parameter. Even with a geometry that would seemingly lead toward cells of aspect ratio 1, for instance for the models of aspect ratio 4 described in the preceding paragraph, cells of aspect 2 are obtained, at least temporarily (see Figure A1).

[28] Two examples of the time evolution of the width of the convective cells and the mean heat flux are presented in Figure 6, at $Ra = 10^6$ and $Ra = 10^8$. The width of the convective cells is computed using the method presented in Appendix A. The correlation between the width of the cells and the heat flux is obvious for the case $Ra = 10^6$. It can be noted that the time periods with cells of width 1 correspond to a smooth evolution of the heat flux, due to the fact that the pattern of convection is in this case quasi-stationary, with a form similar to the one obtained at $Ra = 10^5$ presented in Figure 1, although with narrower plumes. The pattern with two cells of aspect ratio 2 is nonstationary. For $Ra = 10^8$, both patterns are highly nonstationary, but it still appears that wide cells correspond to a low heat flux, whereas narrow cells imply a higher heat flux.

[29] This characteristic has to be taken into account when the method presented in Appendix A is used to construct

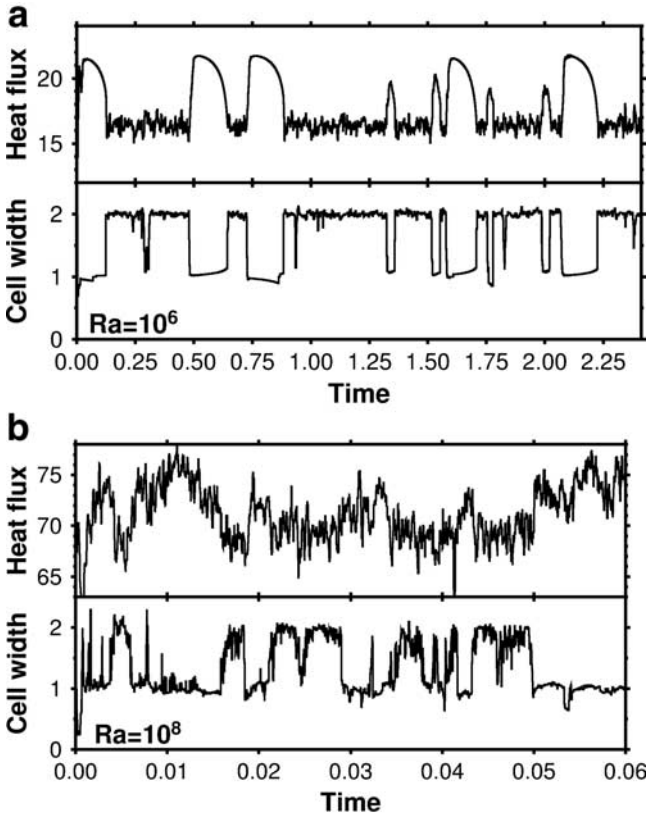

Figure 6. Width of the convective cells and mean heat flux as a function of time, at (a) $Ra = 10^6$ and (b) $Ra = 10^8$. Time and heat flux are nondimensionalized, using d^2/κ as the characteristic time and $k\Delta T/d$ as the characteristic heat flux.

mean synthetic cells of convection. A simple stacking over time of the cases presented in Figure 6 would lead to a mean cell of aspect ratio close to 1.5, with a stacking of cells of width alternatively 1 and 2, and the mean parameters obtained, such as the velocity, the temperature and the heat flux, could be slightly different from the ones obtained for an actual cell of width 1.5. Figure 7 indicates for instance that the heat flux is not a linear function of the cell width L, and a gross averaging over time of cells of different aspect ratios can lead to values of the heat flux not representative of the actual cells observed in the model. In order to be accurate, the method of cells detection and stacking presented in Appendix A must be applied over time periods where the cells keep broadly the same aspect ratio. The stacking then consists mainly in an averaging over time of convective cells of a given width.

[30] The scaling law obtained in equation (21), compared to the one given by *Turcotte and Schubert* [1982, 2002] (equation (18)), and the heat flux obtained in the models of convection, are presented in Figure 7. The values observed (circles) are either the ones directly obtained when a stationary state of convection is achieved at low Rayleigh numbers, or the ones computed using an averaging over time when a statistically stationary state is reached at high Rayleigh numbers. In Figure 7, the scaling laws using the parameter λ as a constant are drawn with dashed and dash-dotted lines. The width λ cannot be larger than the half width of the model (see Figure 5), and for narrow cells, one tends toward a linear profile of vertical velocity, corresponding to the case $\lambda = L/2$. The new computation of the buoyancy force compared to the scaling law by *Turcotte and Schubert* [1982, 2002] clearly gives a mean heat flux closer to the actual values obtained. Best fits are obtained for decreasing values of λ with increasing Rayleigh numbers. For cells of large aspect ratios ($L \geq 2$), a deviation is observed between the model curves and the numerical results, particularly visible for the case $Ra = 10^5$ and $L = 3$. This is due to the fact that the pattern of convection for the large model used here (box of aspect ratio 6) is not a true cell of convection: more than one downwelling and one upwelling are present in the model. As on Figure 2 for the case $Ra = 10^8$ and $L = 2$, cold downwellings (respectively upwellings) start to form at a distance from the central upwelling (downwelling) smaller than the width L of the mean cell. The scaling law proposed in section 2 was built up with the assumption that a steady state loop model could fit statistically time-dependent convection. At high Rayleigh numbers, convection is highly nonstationary and our scaling law still fits well the obtained heat flux. This confirms the result obtained by *Hansen et al.* [1992], about the good agreement between models of stationary convection obtained through steady state equations and time-dependent convection in a statistical sense.

[31] This loop model is relatively successful in predicting the mean heat flux, but a strong restriction is that the horizontal velocity given by equation (15) seems too high compared to the observed values. Figure 8 shows the scaling law for the horizontal velocity given by equation (15) and by the loop model by *Turcotte and Schubert* [1982]. The new scaling law is closer to the observed values, but fits the data only if we consider values of the parameter λ smaller than the ones used to obtain a good fit for the heat flux scaling. The horizontal velocity plotted is the maximal one seen on the horizontal boundaries of the mean synthetic cell obtained with the method presented in Appendix A. It could then be supposed that a part of the discrepancy lies in the method used to construct mean convective cells and thus to measure the horizontal velocity. However, the discrepancy already exists at $Ra = 10^5$, for which convection is stationary and for which the synthetic cells are exactly equivalent to the instantaneous cells observed in the model.

[32] Using equation (3) to compute the mean heat flux as a function of the horizontal velocity u, a better fit is obtained if the velocity given by equation (15) is used rather than the actual horizontal velocity observed. It is also to be noted that the half-space cooling model, which yields the heat flux given by equation (2), is broadly correct in reproducing the form of the heat flux far from upwelling and downwelling currents, but presents some strong discrepancies with the observed spatial distribution of heat flux. The first discrepancy was already noted by *Jarvis and Peltier* [1982, p. 404], who indicated that "the overall effect of the surface is to produce a surface heat flow which is greater than that predicted by boundary layer theory to the left of the center and less than predicted to the right", so that the form of the heat flux given by equation (2) is already only approximate. The second and more important discrepancy lies in the fact that, in order to obtain a correct mean heat flux, the horizontal velocity to be used leads to a heat

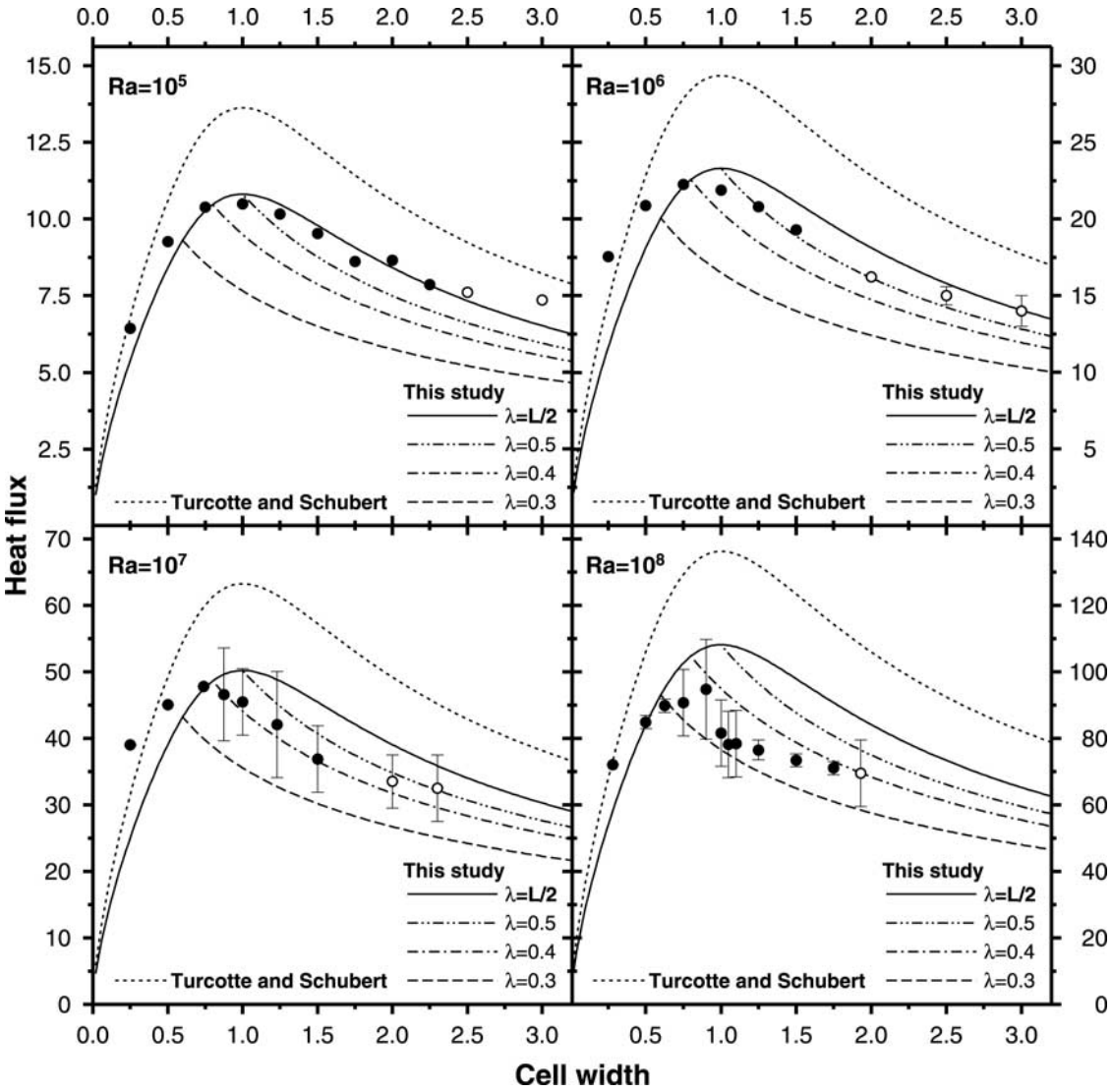

Figure 7. Heat flux as a function of the width of convective cells L, obtained by the scaling law of *Turcotte and Schubert* [1982, 2002] and by the scaling law proposed in this study compared to the actual values obtained by computation of full models of convection (circles). See text for the definition of λ. Solid circles are for cases where cell sizes are permanent, whereas open circles correspond to widths which can be reached only temporarily. Error bars lengths correspond to the maximum variations of the heat flux with time. The absence of error bars means that convection is perfectly stationary. Distances L and λ are nondimensionalized using the total depth d of the model.

flux in the middle of the cell obviously lower than the one observed. These two discrepancies are presented in Figure 9.

[33] The fact that the modeled heat flux has to be lower than the one observed in the middle of the cell is required, given the form of the heat flux given by equation (2). This heat flux tends toward an infinite value above the hot plume ($x \rightarrow 0$). A nonnegligible percent of the mean heat flux computed through equation (21) is due to this part of the heat flux distribution above the hot plume. One could then propose a more accurate model for the form of the heat flux, reaching a maximum finite value for $x \rightarrow 0$. This would lead, instead of equation (21), to an equation of the form

$$\overline{q_t} = 2k\ (T_i - T_0)\left(\frac{u^*}{\pi\kappa\ L}\right)^{1/2}(1 - C) \qquad (19)$$

where C would be a positive term introduced to correct the overestimation of the heat flux above the hot plume. However, in order to obtain the observed mean heat flux, a new horizontal velocity u^* would be computed through the loop model, higher than u obtained by the loop model proposed in section 2, whereas the modeled velocity u is already higher than the one observed. This correction could improve the form of the modeled heat flux, but would increase the difference between the modeled and the observed velocity.

[34] This paradox is indicated here to emphasize the fact that the loop model presented in this paper is very simple and cannot be expected to be perfectly accurate or reproduce all the observables in a convective cell. An important limitation of the model is that it considers a uniform

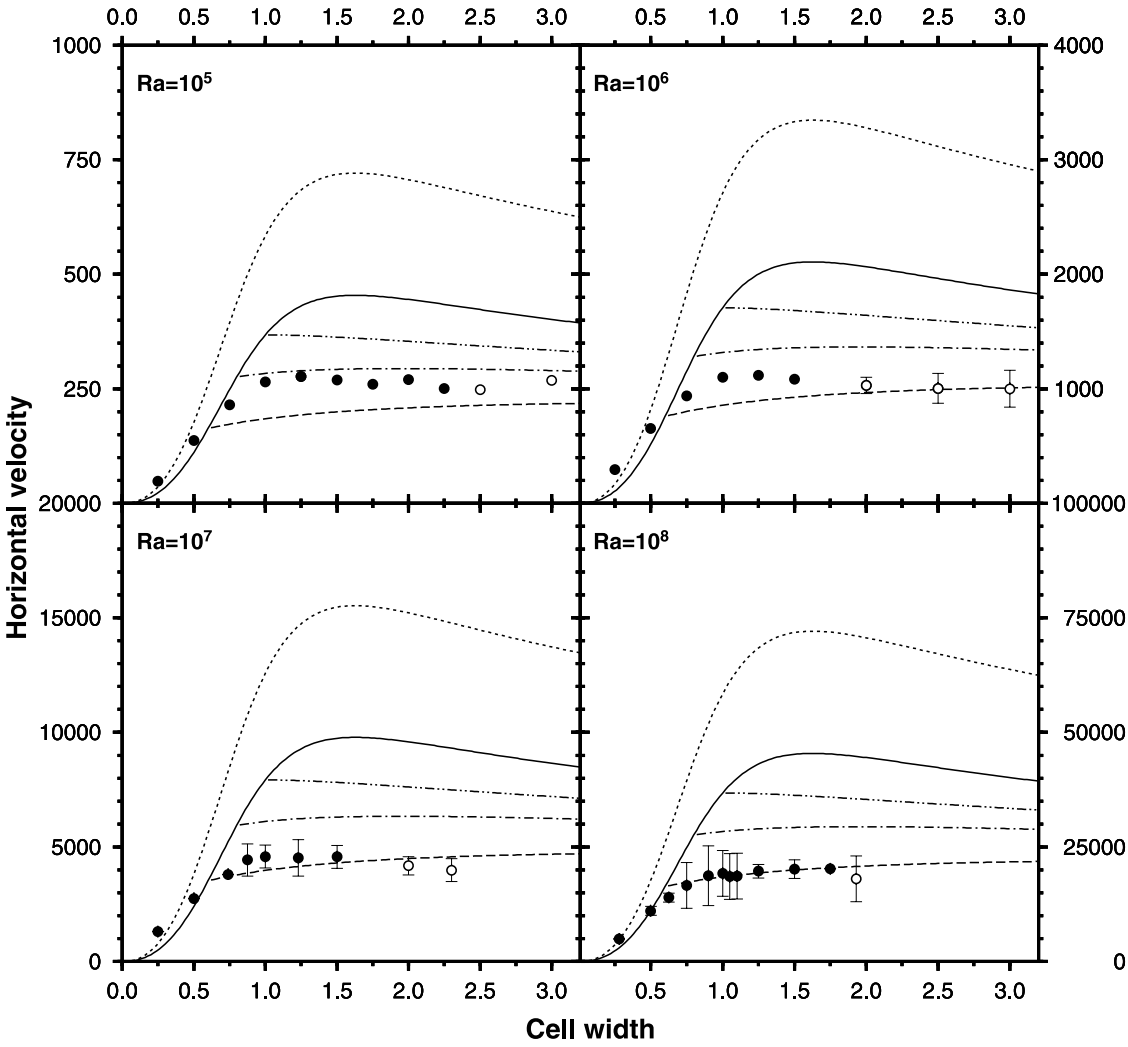

Figure 8. Horizontal velocity on the horizontal boundaries of the model, as a function of the width of convective cells. Notations are the same as in Figure 7. Circles are the maximal observed velocities. The characteristic velocity used for the nondimensionalization is κ/d.

horizontal velocity in the boundary layers, while the observed velocity is a function of x. However, despite its simplicity, this model is relatively successful in predecting the mean heat flux as a function of the Rayleigh number and of the geometry of the convective cells. To write this scaling law, the buoyancy force of the plumes and the shear stress applied to them by the core of the fluid are balanced. Considering only the vertical terms in this equilibrium leads to the relation $Q \sim Ra^{1/3}$. The important point of this loop model is that it takes into account the horizontal shear stress applied to the horizontal boundary layers (equation (10)) as well as the vertical shear stress applied to the plumes. Without this horizontal shear stress, the horizontal velocity, in a dimensionless form, would scale as $u \sim L^{1/3}\lambda^2$, instead of $u \sim L^{1/3}/[L + 1/(8\lambda^3)]^{2/3}$. The horizontal velocity would then increase indefinitely with L. Taking into account the horizontal shear stress is required to explain that the horizontal velocity reaches a plateau with increasing size of convective cells (see Figure 8). For the mean heat flux, the term describing the dependence on the geometry of the cell is $\sqrt{u/L}$, that is to say $\lambda/L^{1/3}$ if the horizontal shear stress is not considered.

[35] It has been proposed that the low-velocity zone under the oceanic lithosphere has a viscosity 1–3 orders of magnitude lower than the rest of the mantle. Consider, for the sake of the discussion, that the horizontal shear resistance then totally vanishes. The loop model by *Turcotte and Schubert* [1982, 2002] considers a linear horizontal profile of vertical velocity, which leads to $\lambda = L/2$. In this case, if no horizontal shear stress appears in equation (12), the dependence of the mean heat flux on the geometry of the cells can be written $Q \sim L^{2/3}$, which means that the heat transfer efficiency increases infinitely with the width of the cells. This mechanism, which could be proposed to explain why the convection in the Earth is of large wavelength, does not hold when one takes into account the fact that the vertical velocity in large cells is of the form of the one presented in Figure 4, instead of a linear profile as proposed by *Turcotte and Schubert* [1982]. The forms of the mean heat flux as a function of the convective cell width, with or

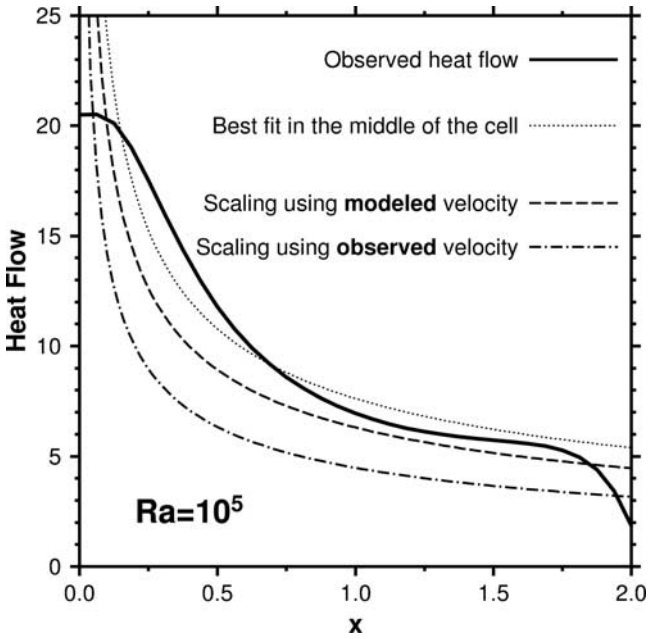

Figure 9. Observed heat flux at $Ra = 10^5$ over a cell of aspect ratio 2, compared to the one given by the scaling law proposed in this paper (dashed line) and to the one given by equation (21) using the observed velocity u (dash-dotted line). The dotted line uses a velocity which gives the best fit with the observed heat flux but leads to a too high mean heat flux.

without horizontal shear resistance, and with a linear profile of vertical velocity ($\lambda = L/2$) or with λ taken as a constant, are presented in Figure 10.

[36] Taking into account the actual form of the vertical velocity is essential to understand that the heat flux cannot increase indefinitely with the size of the cells. The introduction of the horizontal shear stress then does not change drastically the form of the relation $Q \sim f(L)$, but is required to explain the low observed values of the mean heat flux.

4. Heat Transfer in a Plate Tectonic-like Regime

[37] We have seen that the loop model proposed before is in reasonable agreement with the results obtained in classical Rayleigh-Bénard convection. However, the range of length scales that is attainable in such a system is limited to values much smaller than the dominant length scale of mantle convection as evidenced by plate sizes. Here, we use the model of convection with self-consistent plate tectonics proposed by *Tackley* [2000] to test the validity of such scaling in a situation closer to that of the mantle. This model uses a temperature-dependent viscosity that stiffens the top boundary layer effectively making it a stagnant lid [e.g., *Davaille and Jaupart*, 1993], and a constant yield stress that allows, in some cases, the lid to break into plates. We performed a systematic investigation of this situation, varying the different control parameters: the Rayleigh number, the nondimensional heating rate H, the yield stress σ_y and the aspect ratio Λ of the two-dimensional computational domain. The total viscosity contrast is kept constant equal to 10^5, which is enough to put the system in the stagnant lid regime in the absence of yield stress [e.g., *Solomatov*, 1995]. Depending on the choice of parameters, the system can be in this regime or, if the yield stress is reached somewhere in the model domain, in a plate-like regime, as described by *Tackley* [2000]. The full results of this study will be reported elsewhere and only some cases in the plate-like regime are used here, in order to test the applicability of the loop model in this regime.

[38] As in the standard Rayleigh-Bénard situation, the solution can be steady or time-dependent, as in the example shown in Figure 11. The cell detection procedure presented in section 3 and in Appendix A is applied here, after some adaptation to the present situation. The method, presented before and based on velocities works for cases with low internal heating (as the one used in this section) but better results (in term of scatter) are obtained here if the detection is performed on downwelling currents only. This method also works in situations with high internal heating.

[39] In addition to time averages, we also compute, for each detected cell, all relevant diagnostics, like the average temperature, surface velocity, surface and bottom heat fluxes and, of course, the cell size, providing a whole set of cells that can be compared to the loop model. This approach can even be used for evolutionary solution, for example going from one set of parameters to another, and it provides tests of theory for all the effective parameters sets encountered on the way. The loop model should apply to transient cells as long as the time needed to change the cell size is long compared to the time for a fluid parcel to circulate the full loop.

[40] In order to use here the loop model developed in sections 2 and 3 here, a few modifications are needed. The averaged temperature T_m here is not bound to be 1/2 anymore since both internal heat generation and temperature-dependent viscosity make this temperature increase compared to the Rayleigh-Bénard case. The heat flux

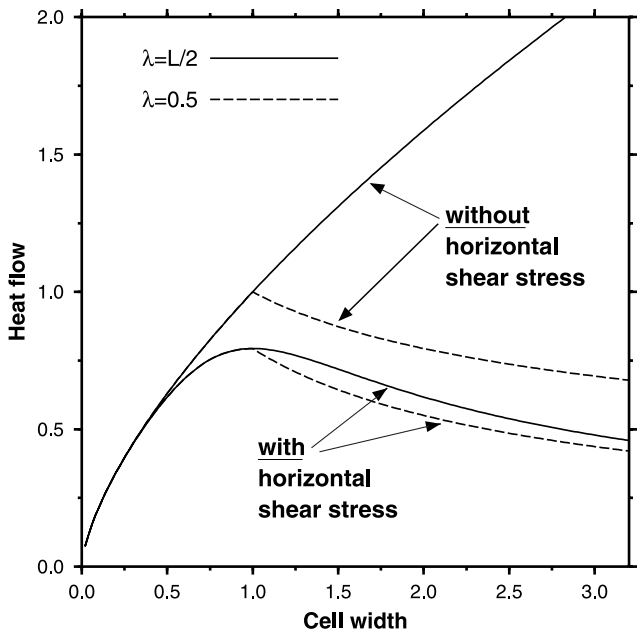

Figure 10. Forms of the heat flux as a function of the convective cell width.

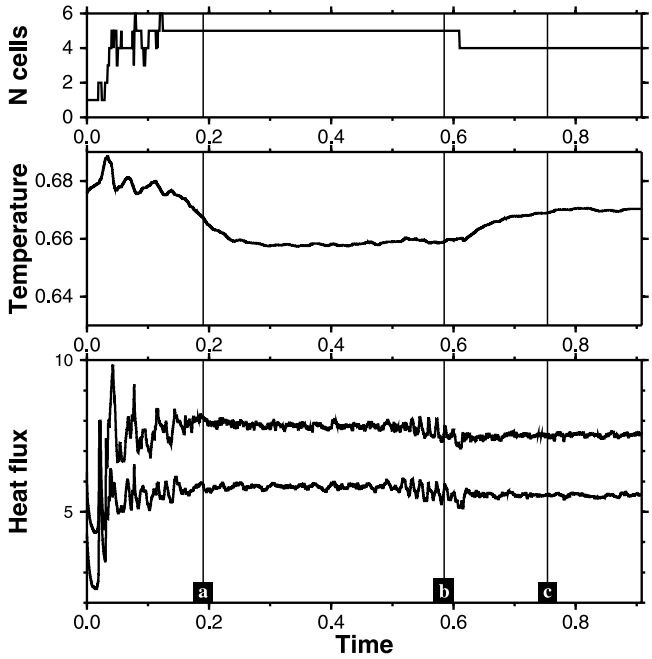

Figure 11. Time evolution of top and bottom (bottom) average heat fluxes, (middle) average temperature, and (top) number of cells in a convective system in the plate-like regime for $Ra = 10^6$, $H = 2$, $\sigma_y = 5.10^4$, and $\Lambda = 32$. The three lines identify the times corresponding to the three snapshots represented in Figure 12.

scaling in such a situation can then be written [*Sotin and Labrosse*, 1999]

$$q = A(L)Ra^{1/3}T_m^{4/3}, \tag{20}$$

and the dependence of the prefactor A on length scale could also be somewhat different because the upwelling flow tends to be less localized in plumes than the downwelling flow [e.g., *Sotin and Labrosse*, 1999]. However, the existence of plates helps localize the upwelling flow, although still less than downwelling ones are, as can be seen on Figure 12. It can then be hoped that $A(L)$ follows roughly the same trend as the one obtained for the simpler situation with no internal heating and an isoviscous fluid, where downwelling and upwelling currents are symmetrical.

[41] In order to test this possibility, we compute, for each cell, either instantaneous or time-averaged, the value of $q/(Ra_m^{1/3}T_m^{4/3})$ and plot all values against the plate (cell) size. Ra_m is the Rayleigh number defined using the viscosity at the temperature T_m, that is the viscosity of the central part of the loop. This is the relevant viscosity since it is the one equilibrating the buoyancy force on the side of plumes. This parameter is an output of the model whereas the Rayleigh number that is imposed as input parameter is defined with the bottom boundary viscosity.

[42] Figure 13a represents the coefficient of the heat flux scaling law as a function of plate size for all cells detected in a time-dependent system corresponding to Figure 11. As shown in Figure 13a, the time evolution displays cells of widely different sizes, even coexisting at each given time (see Figure 11 and the corresponding different symbols in Figure 13a), which nicely allows the loop model to be tested, the predictions of which are also represented for three different values of the parameter λ (0.3, 0.5, and 1, see equation (21)). One can easily see that the prediction of the loop model satisfactorily fits the results for that case. Similar results have been found for the other cases in the plate like regime that have been tested.

[43] The rather large scatter observed for small plate size is due to the fact that the corresponding cells are the transient small cells that exist between the two subduction zones that merge at $t \simeq 0.6$. Two such cells can be seen at $x \sim 19$ on the second snapshot of Figure 12. These cells are very unsteady and the velocity of plate boundaries, just before merging, becomes as large as the fluid velocity, rendering the loop model inappropriate for particular cells. However, after binning all the points corresponding to the cells on intervals of 0.5 in length (Figure 13b), one can see that the average is correctly fitted by the loop model.

[44] The loop model and the full calculation also seem to diverge for very large cell sizes, and several reasons can be invoked to explain that. Dynamically first, it can be expected that small scale convection could start under large aspect ratio cells [*Davaille and Jaupart*, 1994; *Dumoulin et al.*, 2001; *van Hunen et al.*, 2003], rendering the conduction profile assumed for the boundary layer slightly inaccurate for large plates. This explanation does not seem to hold for the case presented here (Figure 12), possibly because the Rayleigh number is not large enough yet. On the other hand, upwelling plumes exist and the flow is not strictly cellular. One has to realize that the loop model is very simple and should not be expected to give a perfect fit to the full dynamical calculation, particularly in the case presented here, with internal heating and a complex rheology.

[45] In addition to instantaneous cells, we represent, in Figures 13a and 13b, the heat transfer coefficient for average cells. The large empty circle is obtained for the cell that is an average over all detected cells. However, the distribution of cell size is not unimodal (see Figure 13c) and averaging the cells separately over the four modes that can be identified on Figure 13c give four different values, represented by empty squares in Figures 13a and 13b, that follow the loop model as well as the individual cells.

[46] Overall, the agreement between the loop model and the results of the full dynamical calculation is rather good, even though the loop model was designed for a somewhat different situation. This means that the basic physics is well captured by the loop model: the coefficient $A(L)$ of the heat flux scaling law presents a maximum at $L \simeq 1$ because the conductive cooling of the boundary layer becomes inefficient when the thickness of the boundary layer is too large.

5. Implications for the Earth and Discussion

[47] Convection in Earth's mantle is of long wavelength, with broadly four cells of convection, of aspect ratio approximately 3. Our model for the heat flux as a function of convective cell size (equation (21)) predicts a mean heat flux for cells of aspect ratio 3 ranging from 55% ($\lambda = 0.5$) to 60% ($\lambda = 0.3$) of the one obtained for cells of aspect ratio 1. This important reduction can help to resolve the problem of

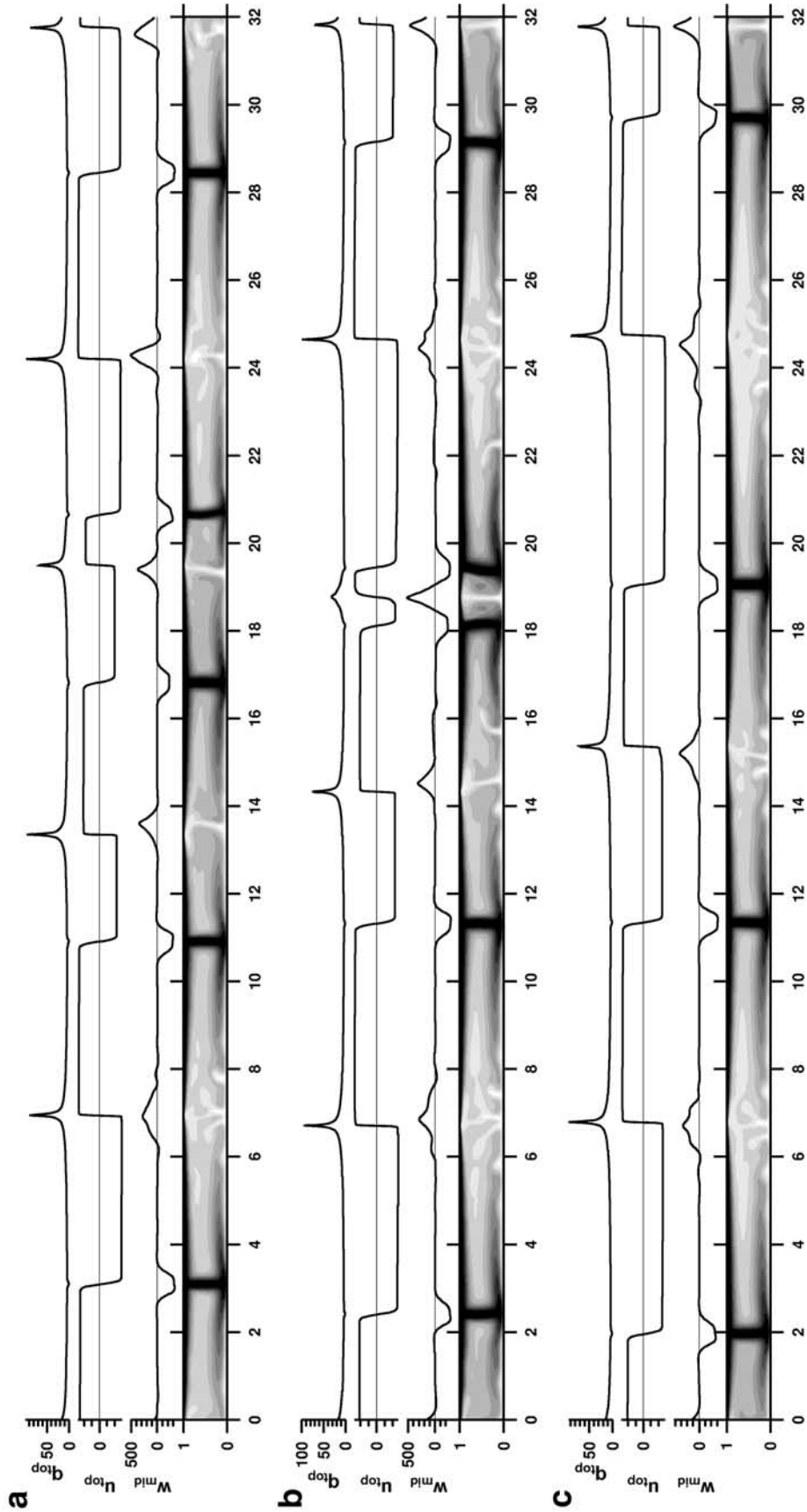

Figure 12. Three snapshots of temperature (bottom), vertical velocity at middepth (w_{mid}), horizontal velocity at the surface (u_{top}) and heat flux (q_{top}) corresponding to the three lines represented on Figure 11.

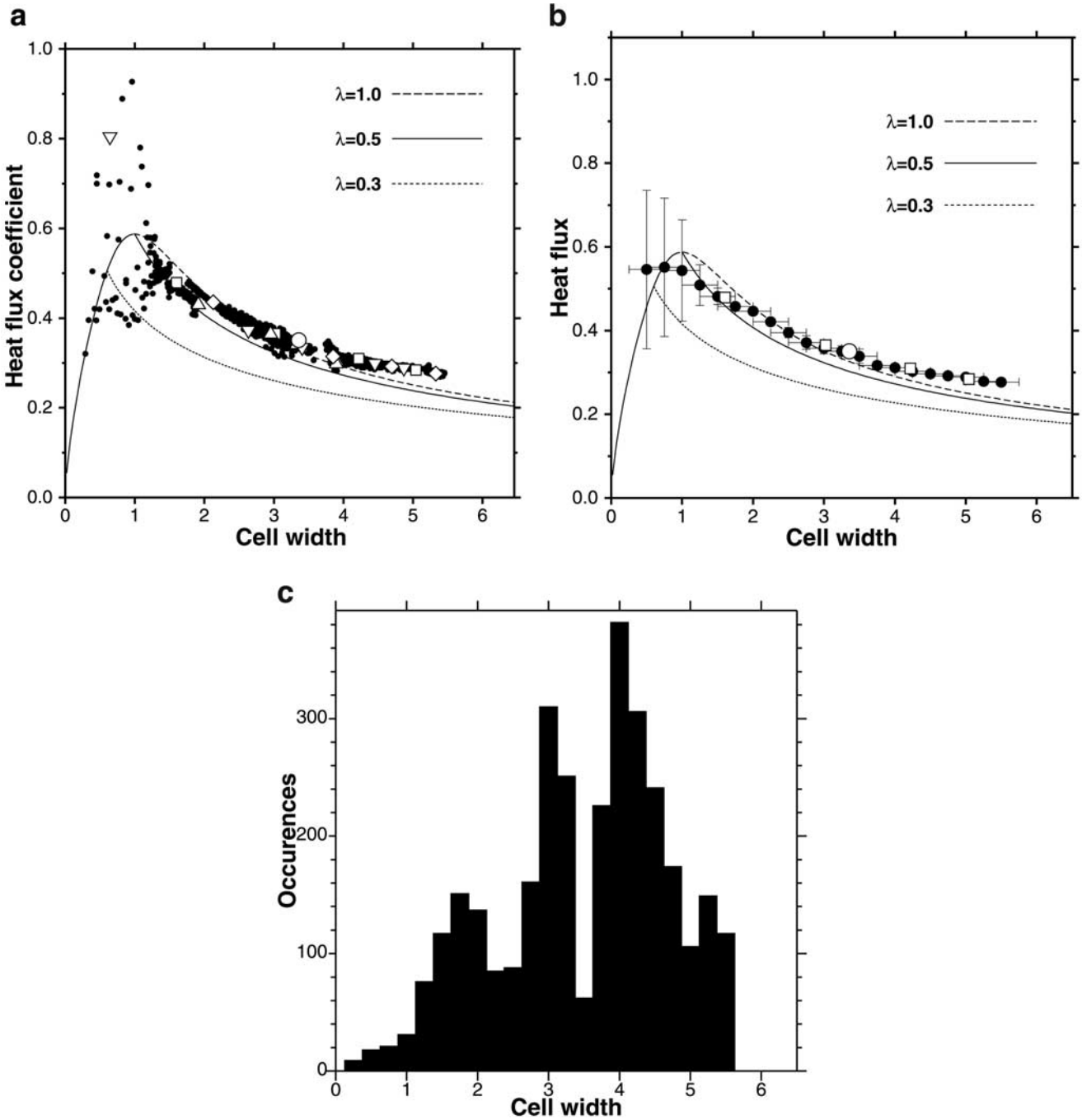

Figure 13. Prefactor for the heat flux scaling law as a function of plate (cell) size during a time evolution corresponding to Figure 11. (a) Each solid circle is the value of $q/(Ra_m^{1/3}T_m^{4/3})$ against plate size for one detected cell at one particular time. (b) Large solid circles result from a moving average over the values of Figure 13a, with error bars representing the interval of averaging and the RMS of fluctuations within it. (c) Distribution of cell sizes. The different lines are the prediction of the loop model for different values of λ (as labeled). Large open symbols on Figures 13a and 13b result from particular cells: circle is for the cell averaged on all detected cells, squares are for cells averaged for each mode seen in the distribution ($0 \leq L \leq 2.25$; $2.25 < L \leq 3.5$; $3.5 < L \leq 5$; $5 < L \leq 5.5$), and triangles, inverted triangles, and diamonds are for cells detected at the time corresponding to Figures 12a, 12b, and 12c, respectively.

rapid initial cooling in parameterized models of mantle thermal history.

[48] The mantle circulation can be expected to depend highly on the position of continents at the surface of the Earth. Long wavelengths dominate when continents are aggregated in one supercontinent, whereas shorter cells must be present when continents are more uniformly distributed at the surface, like in the present-day situation. As shown in Figure 6, changes in the size of the convective cells lead to nonnegligible variations in the mean heat flux over time. The cell width on Figure 6 varies only between 1 and 2. If one considers that the present state for the Earth corresponds to the most "separated" one, as far as the position of the continents is concerned, and that only two cells are present when continents are aggregated in one supercontinent, it is possible to imagine variations over time between cells of aspect ratio 3 to cells of aspect ratio close to 7 for whole mantle convection. Our model then predicts variations in the heat flux due only to changes in the width of the convective cells of the order of 50%, with a higher heat flux obtained in the present-day configuration than in the case with one supercontinent.

[49] The reduction of the efficiency of the heat transfer for large cells of convection does not imply that satisfactory models of mantle cooling can be directly obtained by modifying the coefficient C in the relation $Q = C\ Ra^{1/3}$. In a previous study [*Grigné and Labrosse*, 2001], models of Earth cooling were constructed, composed of a mantle cooling model based on the parameterization by *Sotin and Labrosse* [1999], coupled to the core cooling model by *Labrosse et al.* [1997]. The energy conservation for the mantle is written:

$$Q_t = f^2 Q_b + \frac{H}{3}\left(1 + f + f^2\right), \tag{21}$$

where Q_t and Q_b are the nondimensional heat flux respectively at the top and at the base of the mantle, H is the nondimensional heating rate, and f is the ratio between the core and the Earth radii. The heat flux at the top of the mantle is given by equation (21). *Sotin and Labrosse* [1999] showed that the nondimensional temperature T_m can be written as a function of H and Ra: $T_m = (1 + f^{-3/2})^{-1} + C[(1 + f + f^2)/3]^{3/4}\ H^{3/4}/Ra^{1/4}$, where C is a constant depending on f and on the wavelength of convection L. H includes both radiogenic heating and secular cooling $-\partial T_m/\partial t$. The above relation for T_m is thus of the form $T_m = f(-\partial T_m/\partial t, Ra, L, H_{\mathrm{rad}})$, where H_{rad} is the radiogenic heating rate, and can be used to compute the evolution of T_m over time. Equation (21) can then be used to compute the heat flux Q_b at the core-mantle boundary. The inner core formation and growth can be computed over time using the total heat loss of the core. The present-day inner core radius is then the constraint that fixes the choice of the initial state in our model.

[50] If the concentrations in radioactive elements for a depleted mantle are considered, and with a parameterization obtained for cells of aspect ratio 1, this cooling model gives a present-day total heat loss of the mantle of only ~31 TW, lower than the present-day value of 36 TW once the contribution from heat production in the continental crust (6–7 TW) is subtracted [*Sclater et al.*, 1980]. If large cells are considered in the relation $Q = C\ Ra^{1/3}$, a colder initial state for the mantle must be chosen in order to obtain the correct radius for the inner core, and the final state then obtained still corresponds to a too low heat loss.

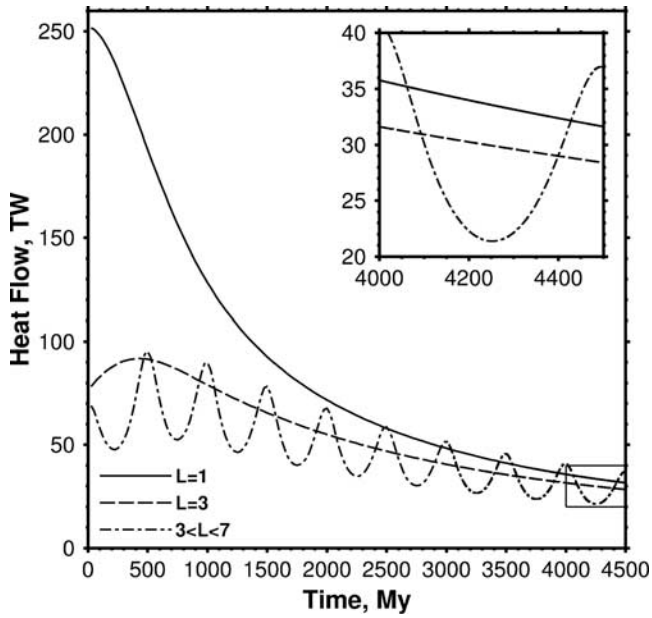

Figure 14. Total heat loss at the surface of the mantle obtained with cells of constant aspect ratios (L = 1 and L = 3) or with cells presenting regular variations between aspect ratios 3 and 7, with a periodicity of 500 Myr. Inset is a focus of the last part of the evolution.

[51] Variations of the wavelength of mantle convection over time can be introduced in this Earth cooling model, by imposing a variation over time of L. Figure 14 presents the total heat loss obtained at the surface of the mantle for the cases of cells of constant aspect ratio, L = 1 and L = 3, and for the case of cells whose width is now 3, and presented in the past variations ranging from $L_{\min} = 3$ to $L_{\max} = 7$, with a constant periodicity of $\tau = 500$ Myr, that is to say:

$$L(t) = L_{\max} + L_{\min} + (L_{\max} - L_{\min}) \cos\left(2\pi \frac{t}{\tau} + a\right), \tag{22}$$

where a is a constant computed so that the present L equals 3 ($a = -53.4$ for $\tau = 500$ Myr). This case must not be considered as accurate for the Earth, but is presented here to emphasize the fact that variations in the size of the convective cells in the mantle can lead to a highly nonmonotonic thermal history of the Earth. It can also be noticed that if the present day corresponds to a "recent" decrease in the size of the cells after the separation of a supercontinent, then the heat flux is presently increasing and reaching a local maximum. Even though the general trend obtained with a model with a varying aspect ratio is close to the one obtained with a fixed aspect ratio, it is important to note that the obtained present heat loss is anomalously high compared to this general trend. It can then be proposed that the present-day estimates for the Earth heat loss correspond to a temporal high anomaly, and may not be explained by

cooling models which consider a monotonic thermal history of the mantle.

6. Conclusions

[52] A scaling law for the mean heat flux out of an isoviscous fluid in Rayleigh-Bénard convection is proposed, based on the same approach as the scaling by *Turcotte and Schubert* [1982, 2002], improved here by the introduction of two modifications. These modifications lead to a better fit between the scaling and the observed values of the heat flux than the former model by *Turcotte and Schubert* [1982].

[53] The long standing problem of the cooling of the Earth, that is the disequilibrium between the heat flow out of the Earth and the heat production by the decay of radioactive isotopes, has often been proposed to be solved by increasing the sensitivity to initial conditions. The most popular way of achieving this is to go against the self regulation implied by temperature dependence of the viscosity [*Tozer*, 1972], using, for example, a smaller exponent in the heat flux scaling with the Rayleigh number [e.g., *Christensen*, 1985; *Conrad and Hager*, 1999; *Yukutake*, 2000; *Korenaga*, 2003]. Another way to increase the sensibility to initial condition is to take into account the growth of continental thermal blankets [*Grigné and Labrosse*, 2001] which, if early enough, allows the initial heat to be conserved for a longer time.

[54] In this paper we presented an alternative solution to the problem of the cooling of the Earth which relies on the fact that the prefactor of the heat flux scaling law strongly depends on the dominant length scale of convective flows. The proposition that the selected pattern of convection is preferentially the one that maximizes the heat transfer efficiency [e.g., *Malkus*, 1954; *Turcotte and Schubert*, 2002] is not supported by the experiments carried out through the present study. In isoviscous models, we could obtain in some cases a periodical transition between large and narrow cells of convection (see Figure 6), with large cells, and thus low heat flux, occurring with a likelihood grossly equivalent to that of cells of aspect ratio one. With a temperature-dependent viscosity in a plate-like regime, large convective cells are more likely obtained, leading to a situation far from a maximal heat transfer efficiency.

[55] In models of convection with self-consistent plates, very long wavelength emerge naturally. The model for the prefactor $A(L)$ proposed in this study, which was built considering an isoviscous fluid, is still satisfactory for this more realistic rheology. The loop model has, however, been shown to diverge slightly from the full dynamical results. No small-scale convection has been observed under the modeled lithosphere to explain this observation, which limits the amount of variation of the heat transfer coefficient as a function of plate size. Such a situation is, however, encountered under old oceanic plates and this should represent a limitation of the present loop model for application to the Earth. Nevertheless, the loop model gives a rather satisfactory fit to the dynamical results.

[56] The main limitation of the model for an application to the Earth is the restricted two-dimensional geometry in which this study was carried out. Even though it can be expected that the convective circulation in the mantle is dominated by the pattern imposed by plate tectonics, that is to say a circulation to first order well represented by a two-dimensional roll pattern of convection, some three-dimensional features, whose importance will have to be quantified, are not taken into account in our models. Further studies will have to include three-dimensional geometry, and the sphericity of the Earth will eventually have to be introduced. However, we can expect that the main physics of heat transfer through thermal boundary layers is well captured by the loop model, and that a change in the geometry of the models will only result in a modification of the form of the prefactor $A(L)$ in the relationship $Q \sim A(L)\ T_m^{4/3} Ra^{1/3}$, with a dependence on the wavelength L broadly similar to the one obtained in a two-dimensional Cartesian geometry, even though the definition of the wavelength L will have to be revised.

[57] The wavelength of convection is a parameter of first importance in the heat transfer efficiency of a convective system. Most scaling laws used in models of cooling of

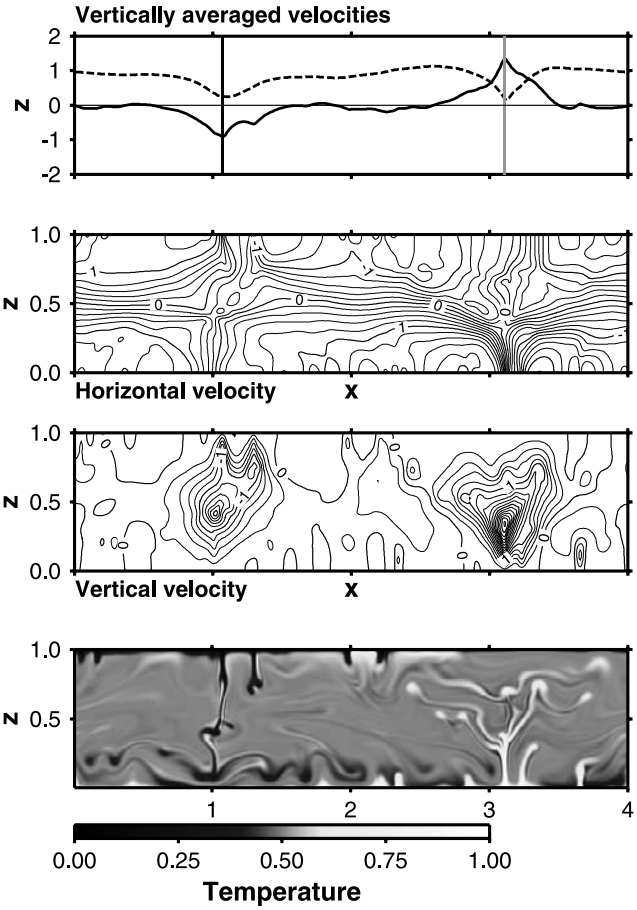

Figure A1. Scheme of the method used in this study to construct stacked convective cells at all Rayleigh numbers. From bottom to top, temperature field, vertical velocity, horizontal velocity, and vertically averaged velocities are shown (dashed line is horizontal velocity; solid line is vertical velocity). This example is for $Ra = 10^8$. Velocities are normalized using the root mean square of the velocity. The detected hot and cold plumes, which define the vertical boundaries of the detected cells, are located at the positions of the light gray (hot) and black (cold) thick vertical lines. Two cells are detected on this example.

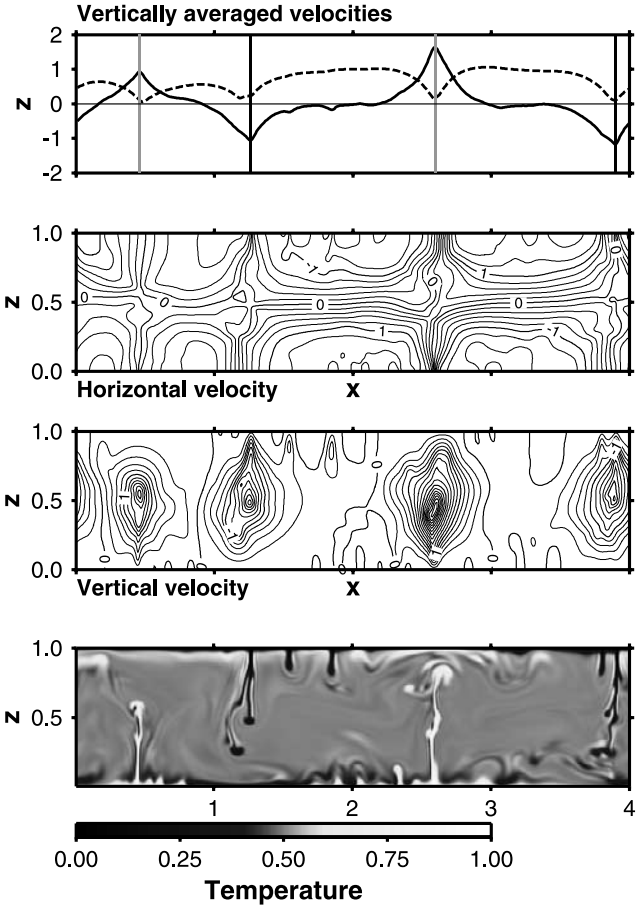

Figure A2. Same as Figure A1, at a different time step, with four cells detected in the model.

terrestrial planets are derived from models of convection of limited width, with most commonly convective cells of aspect ratio one. The important reduction of the heat loss with increasing size of convective cells must be taken into account in models of cooling of planets that display long wavelength features (Earth and Mars), and may help to increase the dependence on initial conditions in thermal history, and slow down the rate of cooling. For the Earth, the variations of the wavelength over time may be fundamental in understanding the thermal evolution of the mantle. On a long timescale, it is possible to imagine variations of the wavelength due to the formation of the continental crust and to the secular evolution of plate tectonics. On a shorter timescale, the Wilson cycle may have a first-order effect. The present situation, with continents well distributed at the surface of the Earth, leads to an abnormally high heat loss compared to a monotonic trend, and therefore cannot be attained by models that do not take into account the variations of wavelength with time.

Appendix A: Mean Synthetic Cells of Convection

[58] We here propose a method to build mean convective cells at all Rayleigh numbers. A cell is defined as the space in the fluid bounded by a hot and a cold plume. At high Rayleigh numbers, plumes move with time, and it is necessary to find a method to locate them. Several methods have been tested. Plumes are zones of abnormally high or low temperature and can then be defined simply with thresholds of temperature. Plumes are also zones on the border of which the gradient of temperature is important. Thresholds on the thermal gradient can also be used to define plumes. These methods can be used to define precisely the position of the plumes and study their dynamics [*Labrosse*, 2002]. However, they only give the locations of the plumes and their whole patterns, which can be very complicated. This approach can not be directly applied to the construction of mean cells of convection.

[59] The purpose of this study is to understand the heat transfer as a function of the length scale of the flow. We thus prefer to work on velocity rather than on temperature. The former is of larger scale and is simpler to use to understand the general circulation in a model. The following method is used: the vertically averaged horizontal and vertical velocities are computed. Zones of downwelling and upwelling correspond to zones where the vertically averaged horizontal velocity is low and the vertical one is peaked. Thresholds are used to determine which zones can be defined as plumes, and the vertical boundaries of the convective cells are located on minima and maxima of the vertically averaged vertical velocity. This method is explained in Figures A1 and A2. Sensitivity to the chosen thresholds is relatively low, the zones of high vertical velocity and low horizontal velocity being generally limited to the real plumes. An accurate choice is for instance to define as plumes, zones where the vertically averaged vertical velocity is above half the total root mean square of the velocity in the model (v_{rms}), and the vertically averaged horizontal

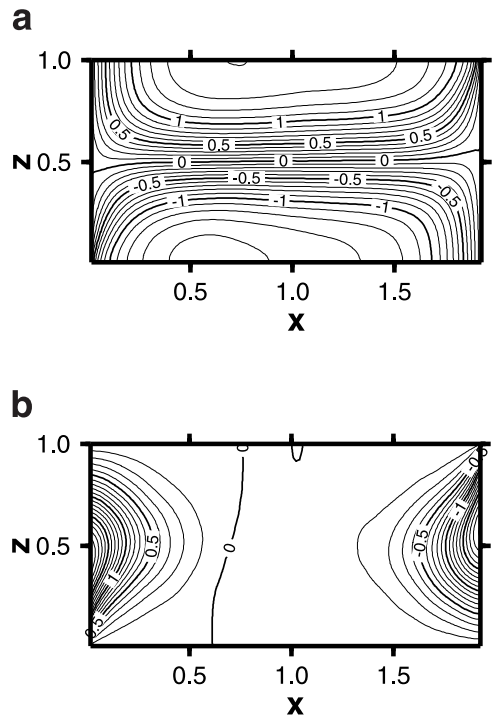

Figure A3. Obtained (a) horizontal and (b) vertical velocities after stacking and computation of the mean cell at $Ra = 10^8$ in a model of aspect ratio 4. The mean cell obtained is of width 2.

velocity is below 0.5 v_{rms}. With this method, only subvertical long plumes are detected. Smaller plumes, attracted toward these larger plumes (see Figure 2) are filtered. The velocity field thus naturally allows to detect the cellular circulations in the model.

[60] Once cells are detected, a position in the cell, defined by the distance between this point and the detected plumes, can be attributed to each point. The different parameters that we intend to study, such as temperature and velocities, are mapped on one mean cell, whose width is the mean width of the different cells detected in the model. At high Rayleigh numbers, for nonstationary convection, the flow varies strongly with time. The mean cells detected in the model are stacked over time, and it is then possible to obtain a mean simple cell of convection for all Rayleigh numbers. The velocities obtained for the mean cell at $Ra = 10^8$ and for a model of aspect ratio 4 are presented in Figure A3.

[61] Varying the width of the model, a large range of cell widths can be obtained. One must, however, keep in mind the fact that with periodic boundary conditions on the vertical walls of the model, the model must contain an even number of cells. As pointed in section 3, the stacking cannot be applied abruptly over time, without taking into account in an accurate way the patterns of convection. Figures A1 and A2 show two configurations obtained for a Rayleigh-Bénard convection at $Ra = 10^8$, one with cells of aspect ratio 1, and the other cells of aspect ratio 2. In such a bimodal case, we separately compute the mean heat flux of cells of aspect ratio 1 and 2.

[62] **Acknowledgments.** We wish to thank Claude Jaupart for helpful discussions. We also thank Francis Albarède, Shijie Zhong, Allen Mc Namara, and an anonymous reviewer for constructive reviews. All figures have been produced using the Generic Mapping Tool of *Wessel and Smith* [1998]. This work was supported by the program "Intérieur de la Terre" of INSU and NSF grant EAR-0229504. This is IPGP contribution 2012.

References

Allègre, C., E. Lewin, and B. Dupré (1988), A coherent crust-mantle model for the uranium-thorium-lead isotopic system, *Chem. Geol.*, *70*, 211–234.

Christensen, U. R. (1985), Thermal evolution models for the Earth, *J. Geophys. Res.*, *90*, 2995–3007.

Conrad, C., and B. Hager (1999), The thermal evolution of the Earth with strong subduction zones, *Geophys. Res. Lett.*, *26*, 3041–3044.

Conrad, C., and B. Hager (2001), Mantle convection with strong subduction zones, *Geophys. J. Int.*, *144*, 271–288.

Davaille, A., and C. Jaupart (1993), Transient high-Rayleigh-number thermal convection with large viscosity variations, *J. Fluid. Mech.*, *253*, 141–166.

Davaille, A., and C. Jaupart (1994), Onset of thermal convection in fluids with temperature-dependent viscosity: Application to the oceanic mantle, *J. Geophys. Res.*, *99*, 19,853–19,866.

Davies, G. (1980), Thermal histories of convective Earth models and constraints on radiogenic heat production in the Earth, *J. Geophys. Res.*, *85*, 2517–2530.

Dumoulin, C., M.-P. Doin, and L. Fleitout (2001), Numerical simulations of the cooling of an oceanic lithosphere above a convective mantle, *Phys. Earth Planet. Inter.*, *125*, 45–64.

Grigné, C., and S. Labrosse (2001), Effects of continents on Earth cooling: Thermal blanketing and depletion in radioactive elements, *Geophys. Res. Lett.*, *28*, 2707–2710.

Gurnis, M. (1989), A reassessment of the heat transport by variable viscosity convection with plates and lids, *Geophys. Res. Lett.*, *16*, 179–182.

Hager, B., R. Clayton, M. Richards, R. Corner, and A. Dziewonski (1985), Lower mantle heterogeneity, dynamic topography and the geoid, *Nature*, *313*, 541–545.

Hansen, U., D. Yuen, and A. Malevsky (1992), Comparison of steady-state and strongly chaotic thermal convection at high Rayleigh number, *Phys. Rev. A*, *46*, 4742–4757.

Honda, S. (1997), A possible role of weak zone at plate margin on secular mantle cooling, *Geophys. Res. Lett.*, *24*, 2861–2864.

Jarvis, G. T., and W. Peltier (1982), Mantle convection as a boundary layer phenomenon, *Geophys. J. R. Astron. Soc.*, *68*, 389–427.

Jochum, K., A. Hofmann, E. Ito, H. Seufert, and W. White (1983), K, U and Th in mid-ocean ridge basalt glasses and heat production, K/U and K/Rb in the mantle, *Nature*, *306*, 431–436.

Korenaga, J. (2003), Energetics of mantle convection and the fate of fossil heat, *Geophys. Res. Lett.*, *30*(22), 2157, doi:10.1029/2003GL018337.

Kraichnan, R. H. (1962), Turbulent thermal convection at arbitrary Prandtl number, *Phys. Fluid*, *5*(11), 1374–1389.

Labrosse, S. (2002), Hotspots, mantle plumes and core heat loss, *Earth Planet. Sci. Lett.*, *199*, 147–156.

Labrosse, S., J.-P. Poirier, and J.-L. Le Mouël (1997), On the cooling of the Earth's core, *Phys. Earth Planet. Inter.*, *99*, 1–17.

Lowman, J., S. King, and C. Gable (2001), The influence of tectonic plates on mantle convection patterns, temperature and heat flow, *Geophys. J. Int.*, *146*, 619–636.

Malkus, W. V. R. (1954), Discrete transitions in turbulent convection, *Proc. R. Soc. London, Ser. A*, *225*, 185–195.

Montagner, J.-P. (1994), Can seismology tell us anything about convection in the mantle?, *Rev. Geophys.*, *32*, 115–138.

Schubert, G., D. Stevenson, and P. Cassen (1980), Whole planet cooling and the radiogenic heat source contents of the Earth and the Moon, *J. Geophys. Res.*, *85*, 2531–2538.

Sclater, J., C. Jaupart, and D. Galson (1980), The heat flow through oceanic and continental crust and the heat loss of the Earth, *Rev. Geophys.*, *18*, 269–311.

Solomatov, V. (1995), Scaling of temperature- and stress-dependent viscosity convection, *Phys. Fluids*, *7*, 266–274.

Sotin, C., and S. Labrosse (1999), Three-dimensionnal thermal convection of an isoviscous, infinite—Prandtl—number fluid heated from within and from below: Applications to heat transfer in planetary mantles, *Phys. Earth Planet. Inter.*, *112*, 171–190.

Su, W.-J., and A. Dziewonski (1991), Predominance of long-wavelength heterogeneity in the mantle, *Nature*, *352*, 121–126.

Tackley, P. J. (1993), Effects of strongly temperature-dependent viscosity on time-dependent, 3-dimensional models of mantle convection, *Geophys. Res. Lett.*, *20*, 2187–2190.

Tackley, P. J. (2000), Self-consistent generation of tectonic plates in time-dependent, three-dimensional mantle convection simulations: 1. Pseudo-plastic yielding, *Geochem. Geophys. Geosyst.*, *1*.

Tozer, D. (1972), The present thermal state of the terrestrial planets, *Phys. Earth Planet. Inter.*, *6*, 182–197.

Turcotte, D., and E. Oxburgh (1967), Finite amplitude convection cells and continental drift, *J. Fluid Mech.*, *28*, 29–42.

Turcotte, D., and G. Schubert (1982), *Geodynamics: Application of Continuum Physics to Geological Problems*, John Wiley, New York.

Turcotte, D., and G. Schubert (2002), *Geodynamics*, Cambridge Univ. Press, New York.

van Hunen, J., J. Huang, and S. Zhong (2003), The effect of shearing on the onset and vigor of small-scale convection in a Newtonian rheology, *Geophys. Res. Lett.*, *30*(19), 1991, doi:10.1029/2003GL018101.

Wessel, P., and W. H. F. Smith (1998), New, improved version of Generic Mapping Tools released, *Eos Trans. AGU*, *79*(47), 579.

Woodward, R. L., and G. Masters (1991), Lower-mantle structure from ScS-S differential travel times, *Nature*, *352*, 231–233.

Yukutake, T. (2000), The inner core and the surface heat flow as clues to estimating the initial temperature of the Earth's core, *Phys. Earth Planet. Inter.*, *121*, 103–137.

Zhang, Y.-S., and T. Tanimoto (1991), Global Love wave phase velocity variation and its significance to plate tectonics, *Phys. Earth Planet. Inter.*, *66*, 160–202.

Zhong, S., and M. Gurnis (1994), Role of plates and temperature-dependent viscosity in phase change dynamics, *J. Geophys. Res.*, *99*, 15,903–15,917.

C. Grigné and P. J. Tackley, Earth and Space Sciences, University of California, 595 Charles Young Drive East, 3806 Geology Building, Box 951567, Los Angeles, CA 900095-1567, USA. (grigne@ess.ucla.edu)

S. Labrosse, Institut de Physique du Globe de Paris, 4 place Jussieu, F-75252 Paris cedex 05, France.